Supplementary Materials

PSMA-targeted extracellular vesicles deliver siADAM9 to suppress tumor progression and enhance androgen-targeted therapy in prostate cancer

Mafewu Olga Raboshakga[1], Anh Duy Do[2], Gwo Harn Max Shiau[3,4], Katsumi Shigemura[5], Chia-Ling Hsieh[4,6], Shian-Ying Sung[1,4,7,8]

[1]International Ph.D. Program for Translational Science, College of Medical Science and Technology, Taipei Medical University, Taipei 11031, Taiwan.
[2]Department of Physiology, Pathophysiology and Immunology, Pham Ngoc Thach University of Medicine, Ho Chi Minh City 700000, Vietnam.
[3]Institute of Biomedical Sciences, Academia Sinica, Taipei 115, Taiwan.
[4]The Ph.D. Program for Translational Medicine, College of Medical Science and Technology, Taipei Medical University, Taipei 11031, Taiwan.
[5]Department of Urology, Kurashiki Medical Center, Kurashiki 710-8522, Japan.
[6]General Clinical Research Center, Chung Shan Medical University Hospital, Taichung 40201, Taiwan.
[7]Department of Medical Research, Chung Shan Medical University Hospital, Taichung 40201, Taiwan.
[8]Institute of Medicine, Chung Shan Medical University, Taichung 40201, Taiwan.

Correspondence to: Dr. Shian-Ying Sung, Institute of Medicine, Chung Shan Medical University, Taichung 40201, Taiwan. E-mail: ssung@csmu.edu.tw; Dr. Chia-Ling Hsieh, General Clinical Research Center, Chung Shan Medical University Hospital, Taichung 40201, Taiwan. E-mail: cshe1539@csh.org.tw

Supplementary Table 1. siRNA sequences and target genes

Target gene	siRNA	Target (5'→3')	Sense/Antisense (5'→3')
ADAM9	siADAM9#1	GCCAGUAUUUAUUGACUCCAAU	Sense: GCCAGUAUUUAUUGACUCCAAU Antisense: AUUGAGCAUCAUAAUACUGGC
	siADAM9#2	CCCAGAGAAAGUCUCCUAUAU	Sense: CCCAGAGAAGUUCCUAUAUAU Antisense: AUAUAUAGGAACUUCUCUGGG
None	siNC	TTCTCCGAACGTGTCACGT	Sense: UUCUCCGAACGUGUCACGU Antisense: ACGUGACACGUUCGGAGAA
FOLH1	siPSMA	CUACUAACAUUACUCCAAAGCAUAA	Sense: CUACUAACAUUACUCCAAAGCAUAA Antisense: UUAUGCUUUGGAGUAAUGUUAGUAG

Supplementary Table 2. RT-qPCR primers for detection and quantification of siRNA

Target	Primer	Sequence (5'→3')
siADAM9#1	Forward	ATTGAGCATCATAATACTGGCG
	Universal reverse	GTGCAGGGTCCGAGGT
	RT	GTTGGCTCTGGTGCAGGGTCCGAGGTATTCGCACCAGAGCCAACGCCAGT

siADAM9#2	Forward	ATATATAGGAACTTCTCTGGGGTT
	Universal reverse	GTGCAGGGTCCGAGGT
	RT	GTTGGCTCTGGTGCAGGGTCCGAGGTATTCGCACCAG AGCCAAACCCCAGA

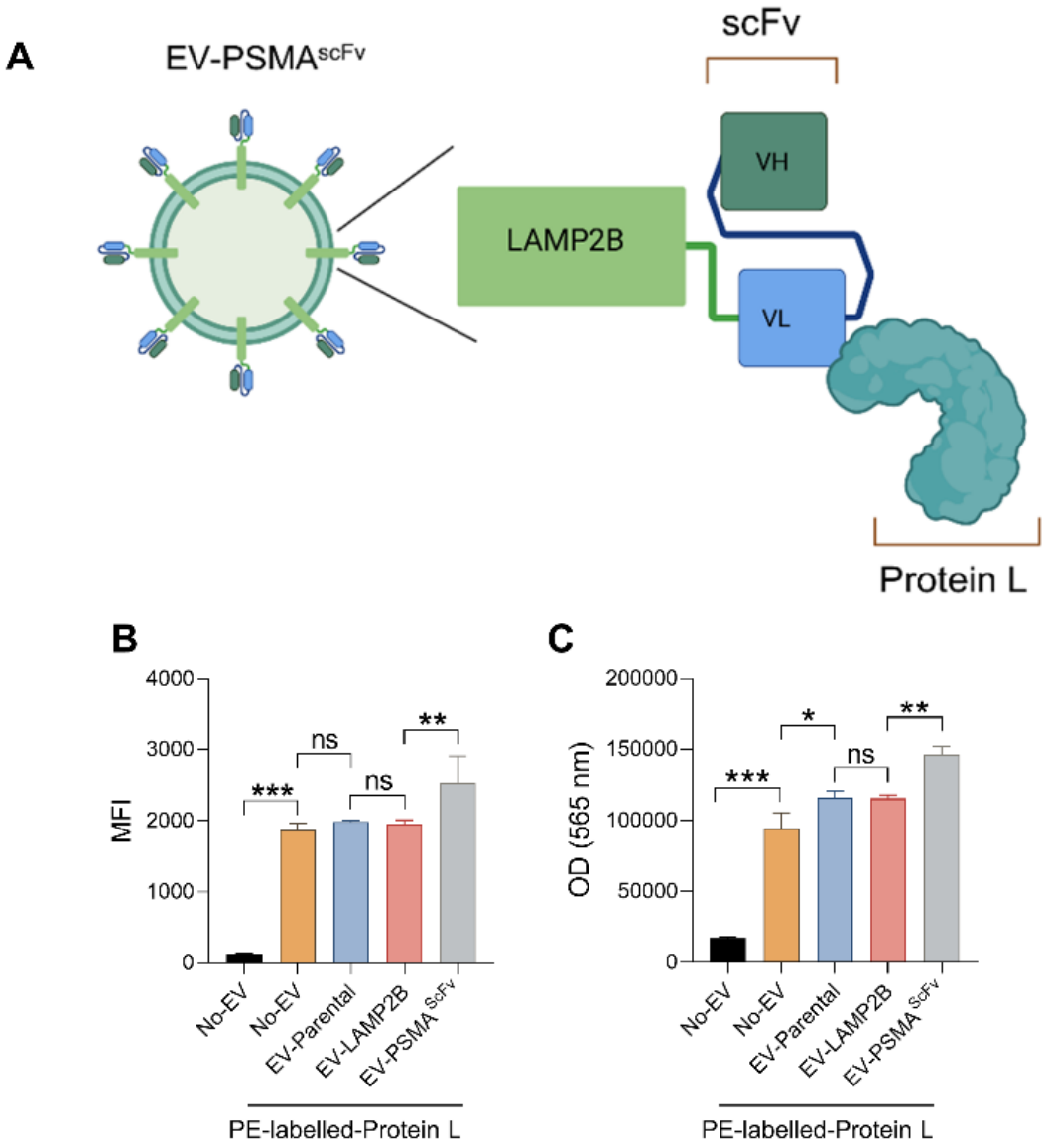
Supplementary Table 3. Antibodies used for western blot analysis

Antibody	**Catalog No.**	**Vendor**
ADAM9	AF939	R&D Systems
AKR1C3	A6229-25UL	Abclonal
anti-goat IgG	705-215-147	Jackson ImmunoResearch
anti-mouse IgG	111-035-146	Jackson ImmunoResearch
anti-rabbit IgG	111-035-144	Jackson ImmunoResearch
β-Actin	GTX109639	GeneTex
AR	sc-816	Santa Cruz Biotechnology
BMI1	#6964	Cell Signaling Technology
BSA	2A3E6	Santa Cruz Biotechnology
Calnexin	#2433	Cell Signaling Technology
CD63	10628D	Thermo Fisher Scientific
CD81	sc-7637	Santa Cruz Biotechnology
CD9	sc-59140	Santa Cruz Biotechnology
CD90	#13801	Cell Signaling Technology
E-cadherin	#3195	Cell Signaling Technology
FLAG tag	F3165	Sigma
HSP70	sc-32239	Santa Cruz Biotechnology
IgG Isotype Control	MAB002	R&D Systems
Lamin A/C	10298-1-AP	ProteinTech
LAMP2	GTX103214	GeneTex
MMP2	#40994	Cell Signaling Technology

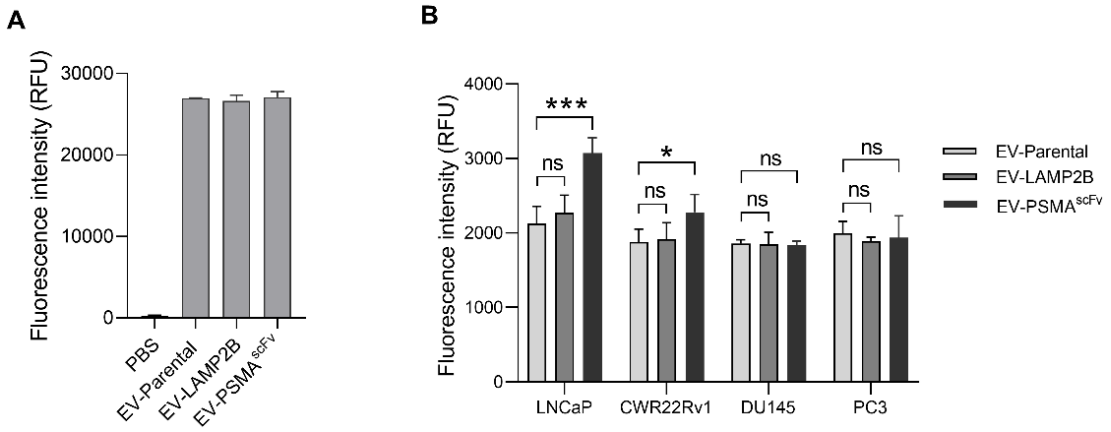
MMP9	#13667	Cell Signaling Technology
N-cadherin	33-3900	Invitrogen
Oct4	GTX627419	GeneTex
p21	GTX629543	GeneTex
Sox2	GTX101507	GeneTex
TIMP3	AF6216G	R&D Systems (Bio-Techne)
TSG101	#72312	Cell Signaling Technology
UBN2	57-194	ProSci
Vimentin	GTX100619	GeneTex

Supplementary Table 4. Primer sequences for gene expression analysis

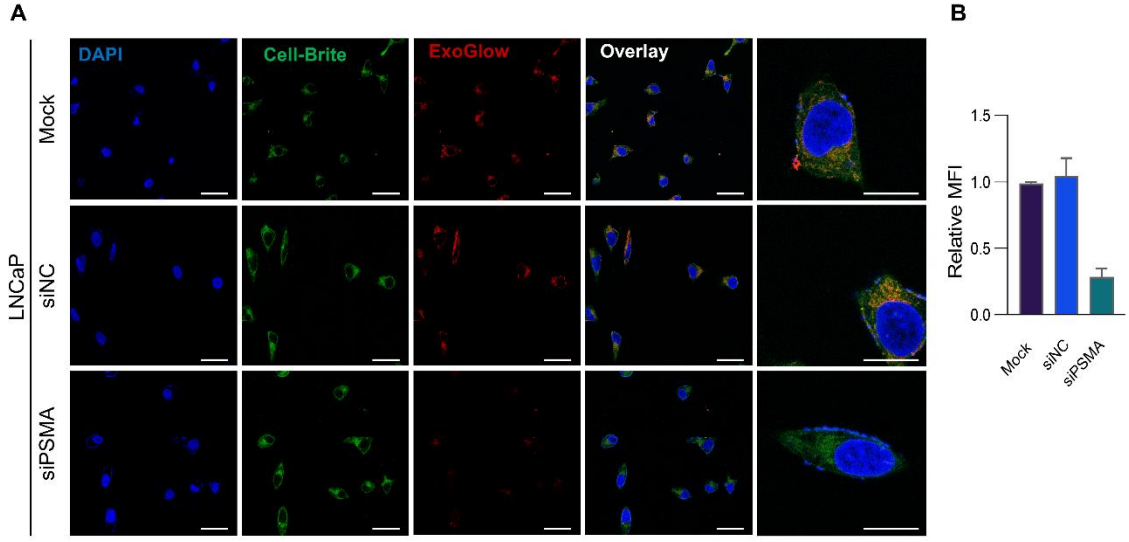
Gene	**Forward Primer (5'→3')**	**Reverse Primer (5'→3')**
ADAM9	GAT GGT TAA CGA AGG CAC	GGC TGT CTA GAA GGG TTT
AKR1C3	CAG TGA TTT TTC TGG GAC TGC	TTC AGC TTG AAA TGG GGA GA
Bmi1	AAT CCC CAC CTG ATG TGT GT	GCT GGT CTC CAG GTA ACG AA
HSPCB	AGCCTACGTTGCTCACTATTACG	GAAAGGCAAAAGTCTCCACCT
Oct4	CCC TGG TGC CGT GAA GCT GGA GAA GG	TAC TGG TTC GCT TTC TCT TTC GGC CCT G
Sox2	TAC AGC ATG TCC TAC TCG CAG	GAG GAA GAG GTA ACC ACA GGG
UBN2	TGT GGC CTA AGG GCT GGA T	GAA CAC TCC GGC TTT CCT TAA A



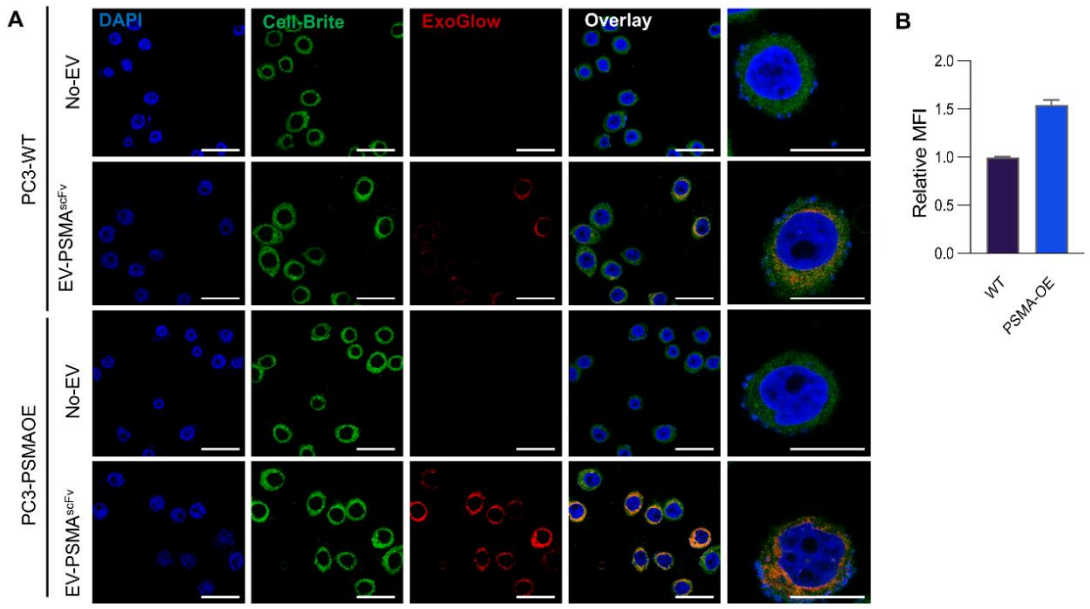
Supplementary Figure 1. Surface presentation of PSMA-scFv on MSC-EVs analysis. (A) Schematic representation of scFv localization and binding to Protein L. Protein L binding to the VH and VL, demonstrating the external topology of PSMA-scFv on the EVs surface; (B and C) Quantitative analysis of EV-PSMA^{scFv} binding to Protein L. Mean fluorescence intensity (MFI) (B) and optical-density (OD) measurements (C) showing the relative binding of PE-Protein L to PSMA^{scFv}, LAMP2B, and Parental MSC-derived EVs, confirming the surface presentation of PSMA-scFv on engineered EVs. The analysis was performed in triplicate across three independent EV preparations (n = 3). Statistical analysis was performed using one-way ANOVA followed by Šídák's multiple-comparisons test. ns, not significant; *P < 0.05; **P < 0.01; ***P < 0.001.



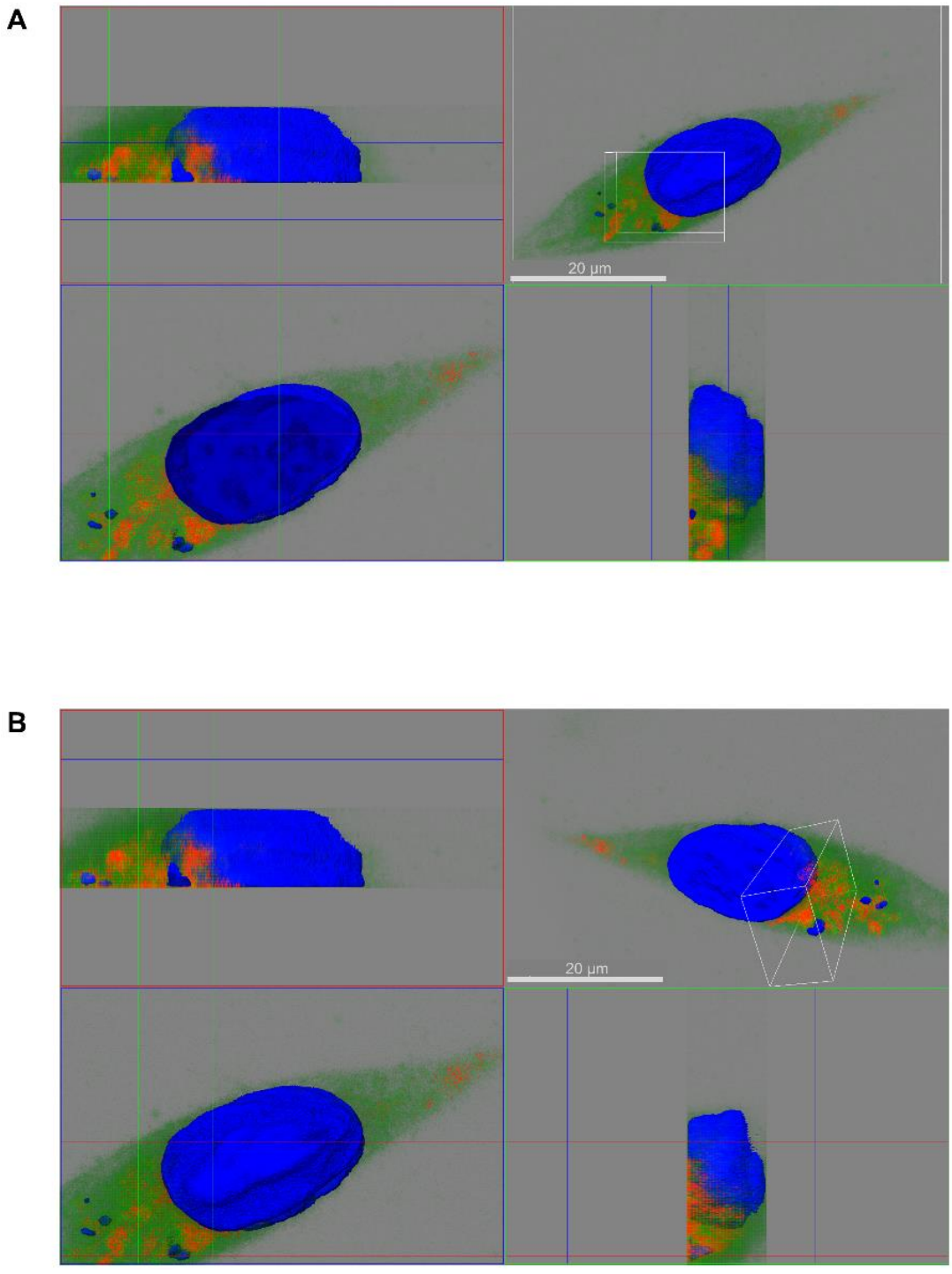
Supplementary Figure 2. Fluorescence-based analysis of EV labeling and binding. (A) Baseline fluorescence intensity of ExoGlow-labeled parental, LAMP2B, and PSMA^{scFv} EVs prior to cell exposure, shown as relative fluorescence units (RFU). PBS containing no EVs was used as vehicle control; (B) Fluorescence-based quantification of the overall cell-associated EV binding in prostate cancer cell lines following incubation with labeled EVs. Experiments were conducted in three independent biological repeats (n = 3), with each repeat using an independently prepared EV batch and analyzed in triplicate. Statistical analysis was performed using two-way ANOVA followed by Šídák's multiple-comparisons test ns, not significant; *P < 0.05; ***P < 0.001.



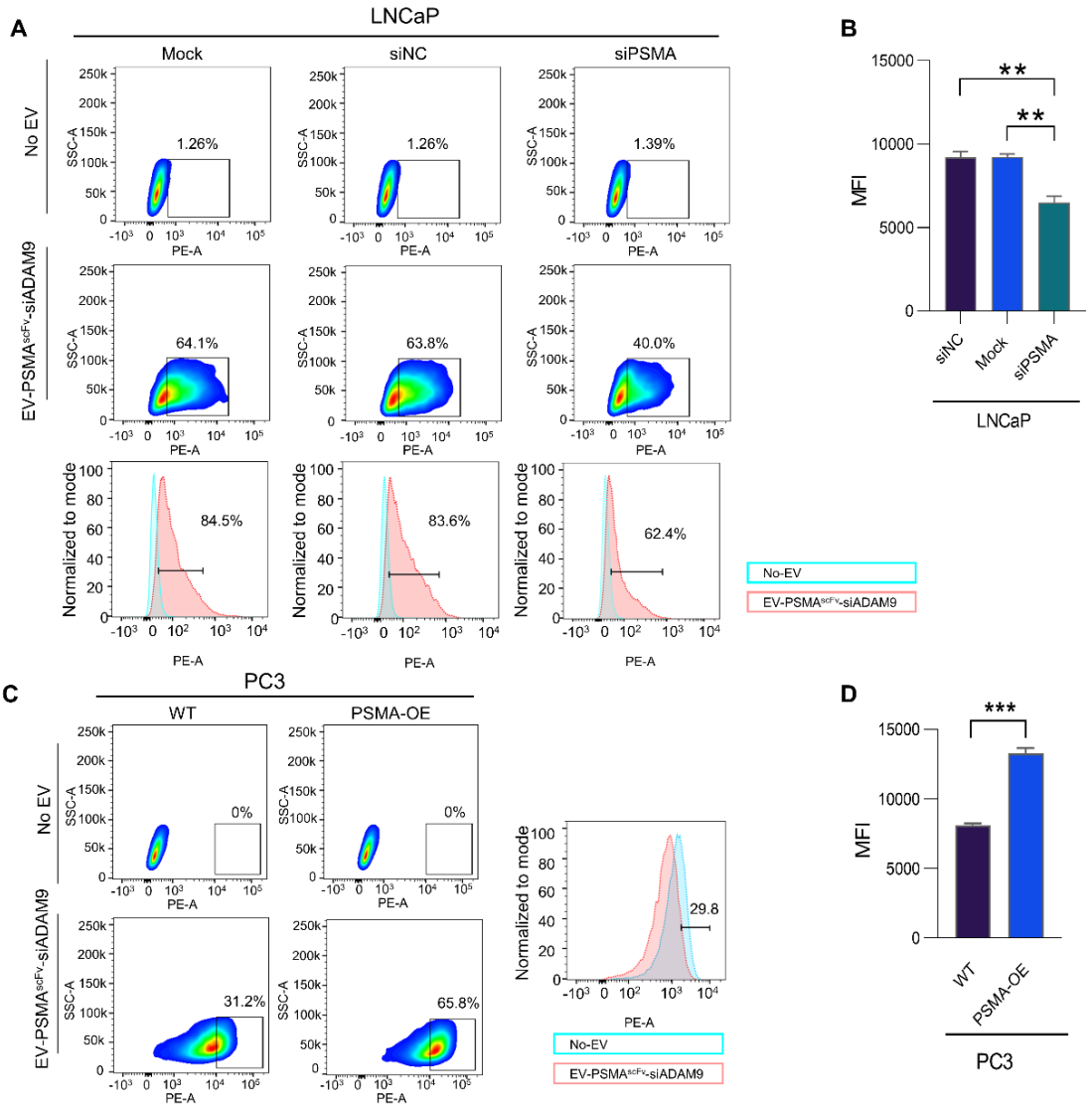
Supplementary Figure 3. EV-PSMA^{scFv}/siADAM9 uptake in PSMA modified LNCaP prostate cancer cells. (A) Confocal analysis of siADAM9 encapsulated EV-PSMA^{scFv} uptake in PSMA knockdown LNCaP prostate cancer cells. Merged and magnified LNCaP cells following coculture with ExoSparkler labelled (red) EV-PSMA^{scFv}/siADAM9. The nucleus (blue) and cell membrane/cytoplasm (green) were stained with DAPI (blue) and CellBrite™ Green, respectably. Scale bars: 40 µM (merged images) and 20 µM (magnified images); (B) Quantification of EV-PSMA^{scFv} fluorescence per cell, in LNCaP-siPSMA, in comparison with controls (mock and siNC). Representative confocal microscopy images and corresponding fluorescence intensity measurements from three fields of view within a single experimental sample using one EV preparation. Data are expressed as mean ± SD.



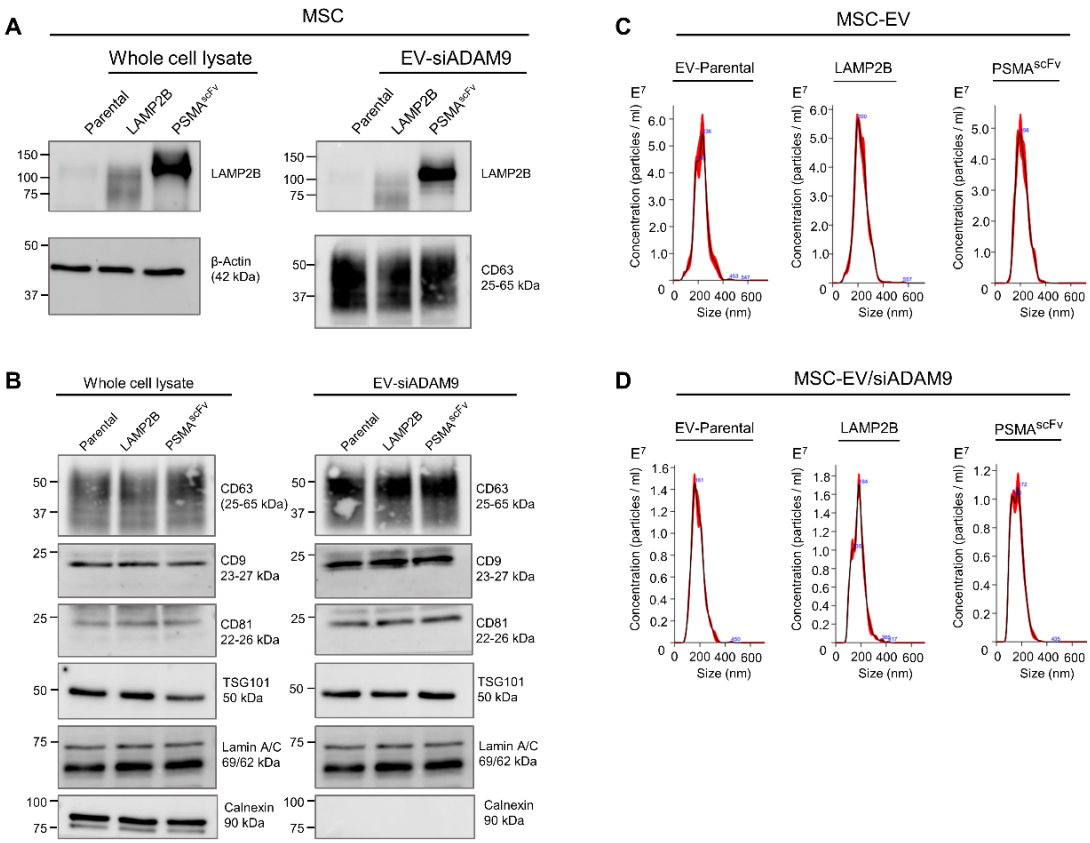
Supplementary Figure 4. EV-PSMA^{scFv}/siADAM9 uptake in PSMA modified PC3 prostate cancer cells. (A) Confocal analysis of siADAM9 encapsulated EV-PSMA^{scFv} uptake in PSMA overexpressed PC3 prostate cancer cells. Merged (A) and magnified (B) PC3 cells following coculture with ExoSparkler labelled (red) EV-PSMA^{scFv}/siADAM9. The nucleus (blue) and cell membrane/cytoplasm (green) were stained with DAPI (blue) and CellBrite™ Green, respectably. Scale bars: 40 µM (merged images) and 20 µM (magnified images); (B) Quantification of EV-PSMA^{scFv} fluorescence per cell, in wild type and PSMA overexpressed PC3 cells. Fluorescence intensity associated with EV treatment was quantified in three microscopic fields from a single experimental sample prepared using one EV batch. Representative confocal images are shown, and data are presented as mean ± SD across the fields of view.



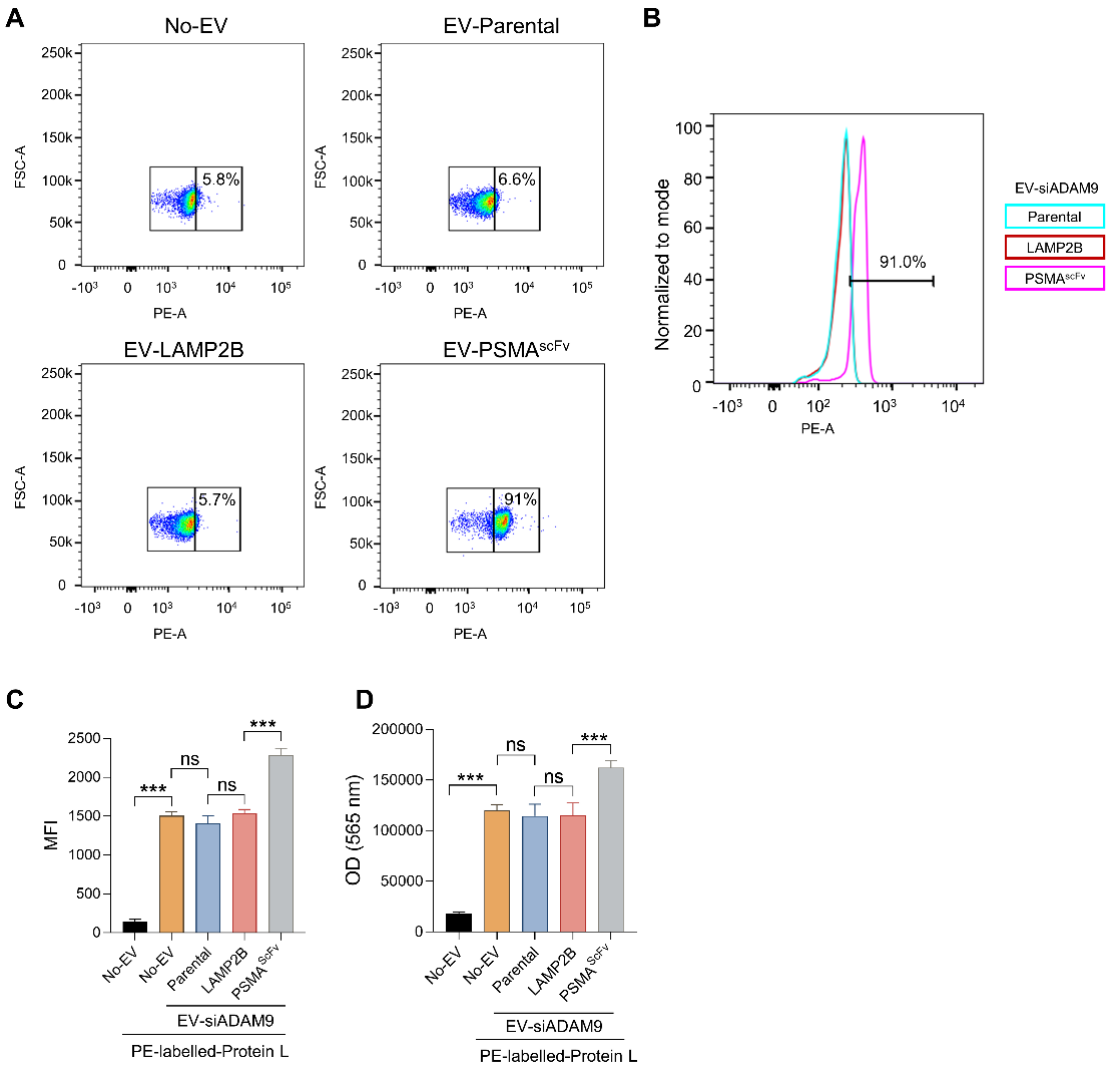
Supplementary Figure 5. 3D confocal Z-stack construction of EV-PSMA^{scFv} uptake in LNCaP prostate cancer cells. A, B: Top (A) and bottom (B) views of a 3D reconstruction of a representative cell showing the intracellular distribution of EV-PSMA^{scFv}, with the selected region of interest (ROI) indicated. Nuclei (blue) were stained with DAPI, membrane/cytoplasm (green) with CellBrite Green, and EVs (red) with ExoGlow. Orthogonal views of the selected ROI along the X, Y, and Z axes are shown. Scale bar: 20 µm.



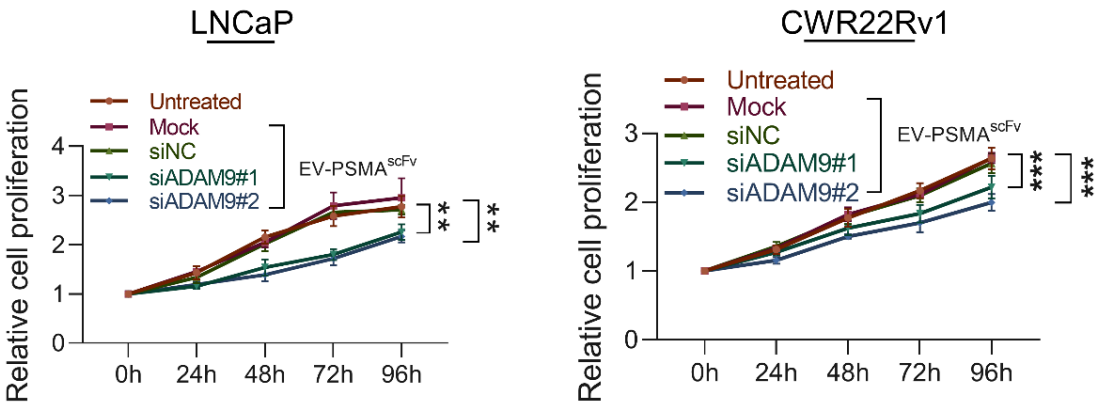
Supplementary Figure 6. PSMA-dependent binding of EV- EV-PSMA^{scFv}-siADAM9. (A and B) Flow cytometric analysis of ExoGlow-labelled EV-PSMA^{scFv}-siADAM9 binding to PSMA-modified LNCaP cells. Representative dot plots and histograms (A) and quantification (B) show EV binding in LNCaP-siPSMA cells compared with mock- and siNC-treated LNCaP cells; (C and D) Flow cytometric analysis of EV-PSMA^{scFv}-siADAM9 binding to PSMA-overexpressing PC3 prostate cancer cells. Representative dot plots and histograms (C) and quantification (D) compare EV binding between PC3-PSMAOE and PC3-WT cells. Representative results are shown from three independent biological repeats (n = 3), each assessed in triplicate with EVs derived from an independant preparation batch. Statistical analysis was done by one-way ANOVA followed by Tukey's multiple-comparisons test (B), and Student's t-test (D). ns, not significant; **$P < 0.01$; ***$P < 0.001$.



Supplementary Figure 7. MSC-EV genetic engineering and characterization. (A and B) PSMA-scFv targeting moiety modification on bone marrow mesenchymal cells derived EVs and proteomic characterization. The immunoblot analysis of PSMA-scFv targeting moiety in whole cell lysate (WCL) and EVs (post siADAM9 encapsulation) in Parental, LAMP2B and PSMA^{scFv} post siADAM9 detected by LAMP2 antibody. β-Actin and CD63 were used as internal controls for WCL and EV fraction, respectively (A). The analysis of EV markers in Parental, LAMP2B and PSMA^{scFv} WCL and EV-siADAM9, per Minimal Information for Studies of Extracellular Vesicles (MISEV) 2023 guidelines; (C and D) Nanoparticle analysis of MSC derived EVs following cargo loading. The size and concentration of EVs (C) and siADAM9 encapsulated EVs (D), comparing the Parental, LAMP2B and PSMA-scFv EVs. Results were obtained from three independently prepared EV batches (n = 3). Representative NTA, images are presented, with these analyses conducted in triplicate. Immunoblotting was performed across three independent biological repeats (n = 3), with one analysis per repeat.



Supplementary Figure 8. Surface presentation of PSMA-scFv on MSC-EV-siADAM9 analysis. (A and B) Flow cytometric analysis of PSMA scFv localization and binding to Protein L. Representative dot plots (B) and histogram (C) showing the binding of PE-labelled Protein L to siRNA encapsulated EV-parental, EV-LAMP2 and EV-PSMA^{scFv} following the incubation with CD63 magnetic beads; (C and D) Quantitative analysis of EV-PSMA^{scFv} binding to Protein L. Mean fluorescence intensity (MFI) (C) and optical-density (OD) measurements (D) showing the relative binding of PE-Protein L to PSMA^{scFv} , LAMP2B, and Parental MSC-derived EVs, confirming the surface presentation of PSMA-scFv on engineered EVs. The analysis was performed in triplicate across three independent EV preparations (n = 3). Statistical analysis was performed using one-way ANOVA followed by Šídák's multiple-comparisons test. ns, not significant; *$P < 0.05$; **$P < 0.01$; ***$P < 0.001$.



Supplementary Figure 9. EV-mediated ADAM9 silencing suppresses proliferation of prostate cancer cells. Cell proliferation assays in LNCaP and CWR22Rv1 cells following treatment with EV-PSMA^{scFv} loaded with siADAM9 variants (#1 and #2), non-targeting siRNA (siNC), or unloaded EVs. Relative cell proliferation was assessed at the indicated time points under monolayer culture conditions. Experiments were independently repeated three times using separately prepared EV batches (n = 3), with triplicate measurements performed for each repeat. Statistical analysis was performed using two-way ANOVA. $^{**}P < 0.01$; $^{***}P < 0.001$.